The postearthquake stress state on the Tohoku megathrust as constrained by reanalysis of the JFAST breakout data

Emily Brodsky, Demian Saffer, Patrick Fulton, Frederick Chester, Marianne Conin, Katelyn Huffman, J. Casey Moore, Hung-Yu Wu

AGU PUBLICATIONS

Geophysical Research Letters

RESEARCH LETTER
10.1002/2017GL074027

Key Points:
- The maximum horizontal stress is 28° from the plate motion suggesting stress changes during the earthquake comparable to the ambient stress
- All possible solutions of the data require that the system was in a normal faulting regime 14 months after the 2011 Tohoku earthquake
- Extrapolating the stress state to the fault results in effective friction that is lower averaged during all of slip

Correspondence to:
E. E. Brodsky,
brodsky@ucsc.edu

Citation:
Brodsky, E. E., D. Saffer, P. Fulton, F. Chester, M. Conin, K. Huffman, J. C. Moore, and H.-Y. Wu (2017), The postearthquake stress state on the Tohoku megathrust as constrained by reanalysis of the JFAST breakout data, *Geophys. Res. Lett.*, *44*, 8294–8302, doi:10.1002/2017GL074027.

Received 2 MAY 2017
Accepted 25 JUL 2017
Accepted article online 28 JUL 2017
Published online 26 AUG 2017

The postearthquake stress state on the Tohoku megathrust as constrained by reanalysis of the JFAST breakout data

Emily E. Brodsky[1], Demian Saffer[2], Patrick Fulton[3], Frederick Chester[3], Marianne Conin[4], Katelyn Huffman[2,5], J. Casey Moore[1], and Hung-Yu Wu[6]

[1]Department of Earth and Planetary Sciences, University of California, Santa Cruz, California, USA, [2]Department of Geosciences and Center for Geomechanics, Geofluids, and Geohazards, Pennsylvania State University, University Park, Pennsylvania, USA, [3]Center for Tectonophysics and Department of Geology and Geophysics, Texas A&M University, College Station, Texas, USA, [4]Universite de Lorraine, CNRS, CREGU, GeoResources Lab, Nancy School of Mines, Campus ARTEM, Nancy, France, [5]Chevron Energy Technology Company, Houston, Texas, USA, [6]Japan Agency for Marine-Earth Science and Technology, Yokohama, Japan

Abstract The Japan Trench Fast Drilling Project (JFAST) endeavored to establish the stress state on the shallow subduction megathrust that slipped during the *M*9 Tohoku earthquake. Borehole breakout data from the drill hole can constrain both the orientation and magnitude of the principal stresses. Here we reanalyze those data to refine our understanding of the stress state on the fault. In particular, we (1) improve the identification of breakouts, (2) consider a fuller range of stress states consistent with the data, and (3) incorporate new and more robust laboratory constraints on rock strength. The original conclusion that the region is in a normal faulting regime after the earthquake is strengthened by the new analysis. The combined analysis suggests that the earthquake released sufficient elastic strain energy to reset the local stress field.

Plain Language Summary The 2011 *M*9.0 Tohoku earthquake produced a catastrophic tsunami by moving the seafloor 50 m at the trench. Stress measurements from a borehole that penetrated the fault confirm that this record-breaking slip appears to have released all of the stress that had been stored at the plate by centuries of plate motion. Prior to the Tohoku earthquake, many scientists believed that each earthquake generally released only part of the stress driving the fault. The stress data presented here quantitatively show that at this locale, the shear stress was entirely released.

1. Introduction

Capturing the state of stress in the aftermath of a major earthquake has been a long-term goal of earthquake physics. Recent observations have revealed that extremely large earthquakes may be distinct in releasing nearly all the shear stress over a large region on the fault [*Ide et al*., 2011]. If so, the physics of large earthquakes could be fundamentally different than small ones.

The Japan Trench Fast Drilling Project (JFAST) expedition (Integrated Ocean Drilling Program (IODP) Expedition 343) endeavored to directly measure the stress state on the fault that generated the largest slip ever recorded in an earthquake. The *M*9.0 2011 Tohoku earthquake slipped ~50 m near the trench producing a tsunami with catastrophic consequences for coastal Japan. Thirteen months after the earthquake, near the site of the largest slip, the JFAST expedition drilled into the megathrust (37°56.34′N, 143°54.81′E) (Figure 1). Multiple boreholes at Site C0019 provided core samples, temperature data, and wellbore logs that carried information about the stress state on the fault [*Chester et al*., 2013; *Fulton et al*., 2013; *Lin et al*., 2013; *Ujiie et al*., 2013].

The resistivity images collected in the logging hole (hole C0019B) showed localized failure of the wellbore wall in the form of breakouts. Breakouts are due to the concentration of the far-field stress differences near the cavity walls, and their analysis provides one of the most powerful tools available to capture the in situ state of stress at the time of drilling [*Zoback*, 2007]. In the case of the JFAST drilling, analyses of breakouts indicate the stress state along a subduction megathrust immediately after a great earthquake. While the relationship between breakout azimuths and orientation of the far-field horizontal stresses is straightforward given common assumptions, analysis of breakout widths to estimate absolute far-field tectonic stress magnitudes requires a constitutive model for the substrate and laboratory measurements or proxy data that define

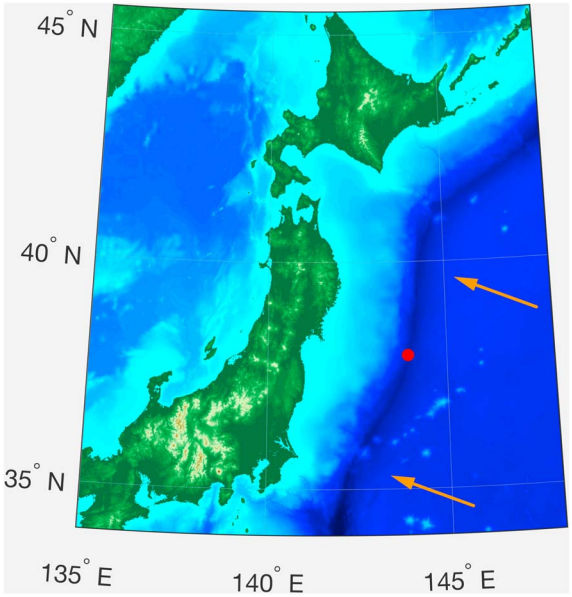

Figure 1. Location map of the JFAST drill site (dot). Arrow indicates plate convergence direction.

rock strength. An early analysis of the borehole breakout data was published immediately after the expedition [*Lin et al*., 2013]. Here we return to this valuable data set in light of new information about breakout identification, rock strength, and uncertainty.

We first reassess the wellbore failures identified in resistivity image data using quality codes that allow us to limit our analysis to the most robustly measured breakouts. We find that the azimuthal direction of the breakouts suggests that the earthquake stress changes were comparable to the background stresses. We then model the observed breakout widths by searching for all possible stress states that would produce the observed breakouts using a fully 3-D failure criterion. Since we do not assume a priori a ratio between the maximum and minimum far-field stresses, we can use the inverted stress state to infer the current shear stress on the fault plane. We then grapple with the mechanical significance of the lack of breakouts within 100 m of the inferred major plate boundary fault at 820 m below the sea floor (mbsf). Finally, we conclude that the borehole breakouts are consistent with complete or nearly complete stress drop during the Tohoku earthquake on the fault at this location.

2. Breakout Identification

Hole C0019B was logged during drilling with Schlumberger Geovision tools [*Chester et al*., 2012]. Breakouts are identified through examination of the resistivity image logs at three different penetration depths into the borehole wall. Because of challenges associated with the very long drill string and extreme water depth of ~7 km, in combination with hole cleaning measures common in nonriser boreholes (drilled using seawater and without mud control), the image quality is only fair and can result in ambiguous breakout identification. Therefore, we assign quality codes based on the clarity of the image (Figure 2). Quality code "Good" indicates vertically extensive and clearly defined breakouts 180° apart (identified by continuous straight dark "stripes" in the resistivity images), which are consistent for multiple penetration depths. Quality code "Fair" indicates a probable breakout that is missing one of the above features. Most often the image is disconnected or the apparent breakout wobbles across a variety of azimuths. Quality code "Poor" indicates a possible breakout. For many poor quality breakouts, we observe a darkened region of the borehole wall on one side, with the opposing side of the borehole wall unclear in the image. For poor breakouts, width is not well defined and therefore they are not used for the stress magnitude calculations.

The final compilation is shown in Figure 3. Breakouts are documented between 575 and 726 mbsf, with the best quality breakouts above 680 mbsf. This independent data set largely agrees with the earlier breakout identification of *Lin et al*. [2013] in what was termed logging Unit IIb (540 to 820 mbsf), but the present work does not identify as many breakouts outside this unit. The breakouts are concentrated in a distinct lithological unit which may be different both in terms of the unit's strength and operational demands on drilling that affected hole conditions. The top of the breakout zone coincides with a distinct change in the resistivity log, and the bottom is a subsidiary fault zone at 720 mbsf [*Chester et al*., 2012]. The main plate boundary fault that slipped in the Tohoku earthquake is identified at 820 mbsf. The expedition science team identified Lithological Units on the basis of logging data. Unit 2 extends from 645 to 660 mbsf, and Unit 3 from 690 to 820 mbsf, but there is no direct lithological information about the breakout zone (logging Unit II) above

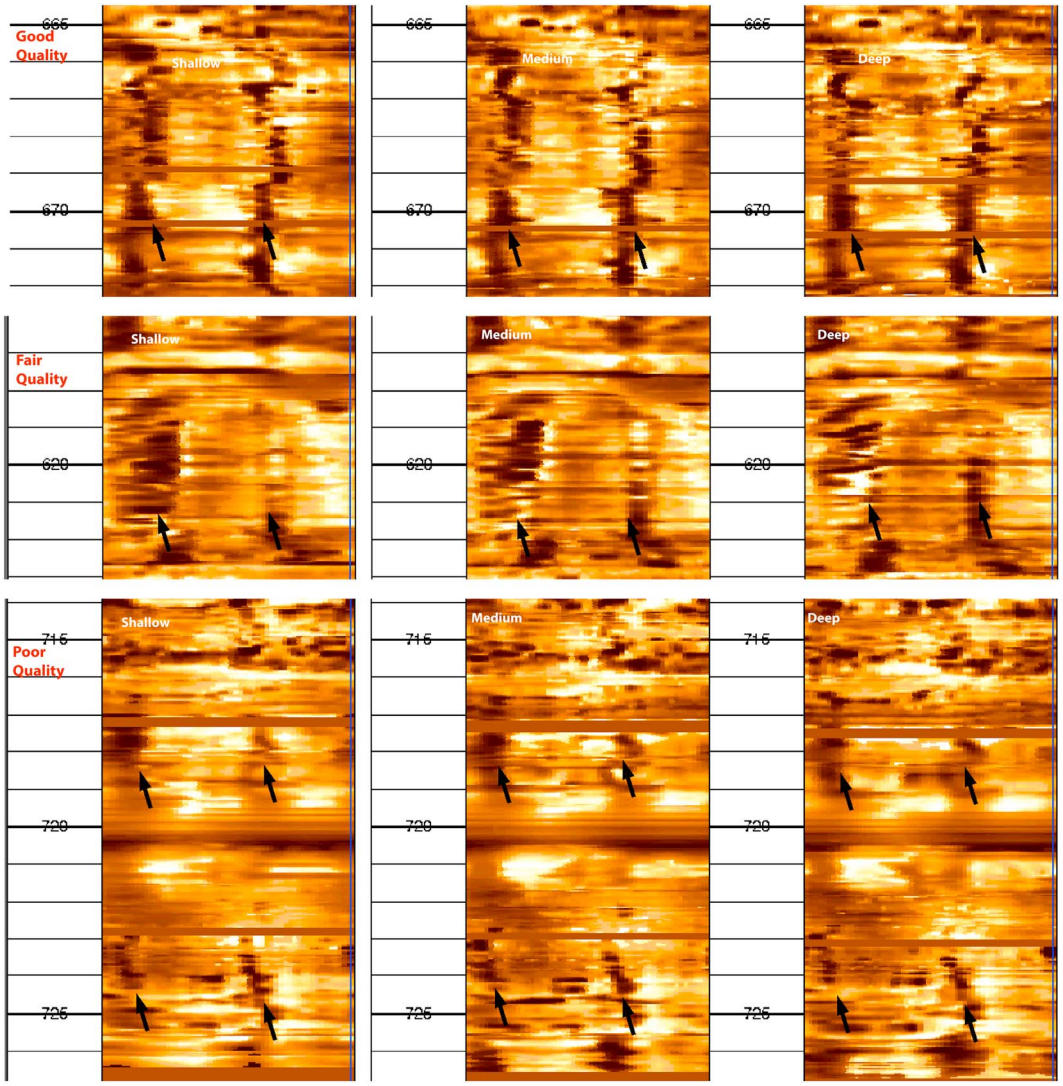

Figure 2. Example breakouts of each quality code. For each row, the quality code is as shown. For each type, three resistivity penetration depths are shown as labeled. Imagery is dynamically processed by CDEX and publically downloadable at http://sio7.jamstec.go.jp/well-logging/343/C0019B/.

645 mbsf or between 660 and 690 mbsf [*Chester et al*., 2012]. The high-quality breakout zone appears to stop near the top of Unit 3. As will be discussed later, the borehole begins its most significant deviation from vertical at the top of this unit and is ultimately inclined by 8°.

The breakouts are somewhat narrower than originally reported in *Lin et al*. [2013], with a mean width of 40 ± 12° (1 SD) (90% confidence interval 20°–59°) for the good and fair breakouts in logging Unit IIb (All confidence intervals in this work are calculated empirically as the limits that encompass the corresponding percent of the measurements.). There is no statistically significant change in width through the ~100 m interval, despite the nearly 20% change in overburden. The mean azimuth is 48 ± 18° (1 SD) (90% confidence interval 19°–76°).

For a vertical well in a stress field with one principal axis vertical, the azimuth of the breakouts is centered on the minimum horizontal principal stress ($S_{h\min}$) [*Zoback*, 2007]. Therefore, the maximum principal horizontal stress ($S_{H\max}$) orientation at the JFAST site at the time of drilling (23–25 April 2012) is interpreted to be 138 ± 18° (90% confidence interval 109–186°). This orientation is similar to that reported in the expedition preliminary report [*Chester et al*., 2012]. The plate convergence direction is 110° (290°) [*Argus et al*., 2011]. Therefore, the alignment of the postearthquake $S_{H\max}$ with the convergence direction is permitted, but

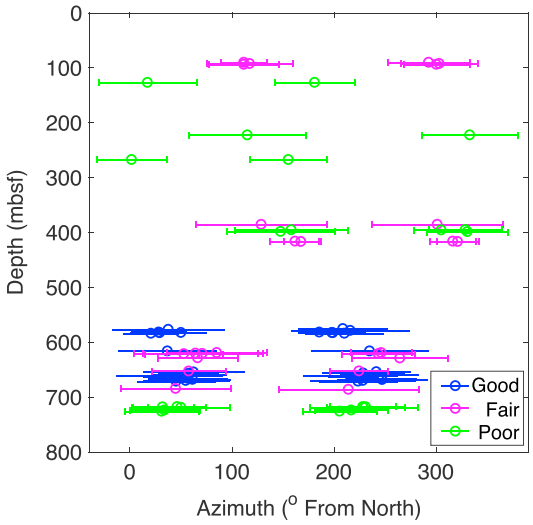

Figure 3. Compiled breakout orientation and width colored by quality codes. Symbols indicate the azimuth at the center of the breakouts, and horizontal bars span the width. Depth is in meters below sea floor (mbsf).

not required by the data. The azimuth of the preferred solution is rotated 28° clockwise from the convergence direction. Note that in steeply dipping strata with strong strength anisotropy, rotation of breakout azimuth away from true stress directions to align with bedding strike can occur if the dip directions of strata are not aligned with $S_{H\max}$ [*Lee et al.*, 2013]. At C0019, the plunge of steeply dipping bedding planes within the depth interval 299–817 mbsf is generally parallel to the convergence direction, consistent with cylindrical folding about an axis oriented 12°, 208.5° and a 95% confidence cone of less than 8° [*Chester et al.*, 2013]. This records shortening at 298°, essentially coincident with the plate convergence direction. The shortening direction of strata at C0019 also is recorded by the anisotropy of magnetic susceptibility (AMS) with a strong preferred orientation of the maximum AMS axes consistent with horizontal tectonic shortening nearly parallel to the convergence direction [*Yang et al.*, 2013]. At C0019 the breakouts do not align with bedding and the convergence direction, so the inferred direction of stress cannot result from a rotation due to strength anisotropy of bedding, and thus, we interpret it to reflect the true direction of $S_{H\max}$.

3. Implication of Breakout Azimuth

Over the long term, it is very likely that the principal stresses are aligned with the plate convergence direction. As discussed above, both discrete structures and ductile fabric in the prism at the borehole are consistent with compression in the plate convergence direction over geological time [*Chester et al.*, 2012]. The occurrence of the earthquake with 50 m horizontal motion nearly E-W also suggests the stress state prior to the earthquake was aligned in the same way. The lack of alignment between the convergence direction and the best fit breakout azimuth at the time of drilling suggests that the earthquake sufficiently perturbed the stress field to change the orientation of the horizontal principal stresses (likely by changing their relative magnitudes). Such a perturbation requires coseismic stress changes on the order of the background stress magnitudes [*Hardebeck*, 2012]. The azimuth data alone favor, but do not require, this relatively large perturbation. As will be discussed below, breakout width provides further evidence.

4. Analysis of Breakout Width

We first interpret the breakouts by doing a grid search of all possible stress states with one vertical principal stress and then finding the combination of far-field stresses that are consistent with the observed breakout widths. This approach considers a slightly broader range of stress states than a stress polygon analysis that limits the maximum ratio of the principal stresses based on an assumed far-field Coulomb failure criterion analyses [*Zoback*, 2007].

Following *Zoback* [2007], we calculate the stress concentration on the borehole wall using the Kirsch equations for horizontal stress states [*Jaeger and Cook*, 1976]. This formulation presumes that upon borehole excavation, the surrounding rocks behave dominantly elastically; this is likely to be valid because even for shallowly buried sediments that undergo plastic yield during burial, the unloading associated with opening of the borehole should result in elastic behavior. Stress orientation and magnitudes are modified in the vicinity of the borehole wall by the presence of the cavity, with the greatest magnitude changes occurring at the

wall. Given principal horizontal solid total stresses $S_{H\max}$ and $S_{h\min}$ and vertical solid stress of S_v, for a vertical borehole the resulting effective principal stresses in the cylindrical coordinate frame of the borehole at the wellbore wall are

$$\begin{aligned}\sigma_{rr} &= \Delta p \\ \sigma_{\theta\theta} &= S + S_{H\max} - 2(S_{H\max} - S_{h\min})\cos(2\theta) - 2P_p - \Delta p \\ \sigma_{zz} &= S_v - 2v(S_{H\max} - S_{h\min})\cos(2\theta) - P_p\end{aligned} \tag{1}$$

where θ is the azimuthal angle from the direction of $S_{H\max}$, P_p is the formation pore pressure, P_p the difference between the borehole and formation fluid pressure, and v is the Poisson's ratio [*Zoback*, 2007]. Because drilling was conducted using seawater, we calculate the hydrostatic fluid pressure with a water density appropriate for the high pressure conditions of the well (1040 kg/m^3). We use a value of 0.4 for Poisson's ratio, which is intermediate between the core sample (0.34–0.40) and seismic data (>0.46) constraints [*Nakamura et al.*, 2014]. The vertical stress is calculated from the overburden, assuming an average rock density of 1740 kg/m^3. The value of Δp is inferred from the difference between the annular pressure measured during drilling and the hydrostat, typically on the order of 6–9 MPa (Logging data with annular pressure measurements are available at http://sio7.jamstec.go.jp/welllogging/343/C0019B/ORIGINAL/DATA/343_C0019B_Run1_MWD_geoVISION.las.).

If the local deviatoric stresses are high enough, failure occurs at the borehole wall. In this paper, we use a three-dimensional failure criterion, the modified Wiebol-Cook, to calculate the fraction of the borehole wall that fails for each possible stress state [*Colmenares and Zoback*, 2002; *Zoback*, 2007]. The failure criterion is

$$J_2{}^{1/2} \geq J_{\text{fail}}{}^{1/2} \tag{2}$$

where the octahedral shear stress J_2 is computed from the principal stresses in the borehole reference frame at each point on the borehole wall according to

$$J_2 = \frac{1}{6}\left[(\sigma_{rr} - \sigma_{zz})^2 + (\sigma_{\theta\theta} - \sigma_{zz})^2 + (\sigma_{rr} - \sigma_{\theta\theta})^2\right] \tag{3}$$

and the failure stress state is given by

$$J_{\text{fail}}{}^{1/2} = A + BJ_1 + CJ_1{}^2 \tag{4}$$

$$J_1 = \frac{1}{3}(\sigma_{rr} + \sigma_{\theta\theta} + \sigma_{zz})$$

with

$$\begin{aligned}A &= \frac{C_0}{\sqrt{3}} - \frac{C_0 B}{3} - \frac{CC_0{}^2}{9} \\ B &= \frac{(q-1)\sqrt{3}}{q+2} - \frac{C}{3}(2C_0 + (q+2)\sigma_3) \\ C &= \frac{\sqrt{27}}{2C_1 + (q-1)\sigma_3 - C_0}\left[\frac{C_1 + (q-1)\sigma_3 - C_0}{2C_1 + (2q+1)\sigma_3 - C_0} - \frac{q-1}{q+2}\right]\end{aligned} \tag{5}$$

and

$$C_1 = (1 + 0.6\mu_i)C_0 \tag{6}$$

Although the algebraic form of the modified Weibol-Cook is much more complex than a Coulomb failure criterion, it is more appropriate for this application because of its use of the full three-dimensional stress field, and in particular because it incorporates the effects of the intermediate principal stress on rock failure. Since failure is determined by the sum of all the differential stresses (the octahedral shear stress), the maximum differential stress is well determined by this formulation.

The key parameters of the Modified Weibol-Cook criterion are the unconfined strength C_0 and the internal friction μ_i. A shipboard unconfined triaxial test was run on a single sample from the breakout zone (714 mbsf) during the drilling expedition, and the maximum failure strength was 3.8 MPa, indicating an upper bound for the unconfined compressive stress (UCS) [*Chester et al*., 2012]. Between the breakout unit and the 820 m fault zone, three tests provided maximum values of 6.4–7.6 MPa. The small number of tests, in combination with the fact that the experiments were conducted under atmospheric conditions and without control of saturation or pore fluid pressure, makes these initial UCS estimates subject to large uncertainty. In particular, partial saturation in clay-rich sediments could lead to erroneously high UCS values. Therefore, we used the additional information now available from multiple friction tests on intact core from 650 to 750 mbsf [*Ikari et al*., 2015]. This study measured values of $\mu_i \approx 0.5$ and cohesion of 0.3–0.4 MPa. The cohesion S_0 is related to the unconfined compressive strength C_0 in the modified Wiebol-Cook criterion by

$$C_0 = 2S_0\left(\sqrt{\mu_i + 1} + \mu_i\right) \tag{7}$$

The resulting values of C_0 from the cohesion measurements data are 1–2 MPa. These values are significantly less than the upper bound from the direct experiment and provide a better estimate of the true UCS; therefore, these are the values we used for our inversion. Since we are interested ultimately in the maximum deviatoric stress possible in the system today, we investigate values with the upper bound values of $C_0 = 2$ MPa and $\mu_i = 0.5$.

For each measured breakout width, we find all possible stress states that are consistent with the observation within the error of the measurements. Based on the pixel size of the image, the measurement error is ±2°. We also identify the optimal stress state as that which minimizes the difference between the predicted breakout width and the observed (Figure 4). Stress states are investigated with a grid search bounded by the physical limits of the stress states. On the lower end, all solid horizontal stresses must be larger than the pore pressure and on the upper end the horizontal stresses are bounded by the unconfined compressive strength added to the vertical stress S_v. Stress states that result in tension in the borehole are rejected because of a lack of any evidence for induced tensile failure [*Chester et al*., 2012]. Based on the relative magnitudes of the two horizontal stresses and the vertical stresses, we then classify each solution as a normal, thrust, or strike-slip regime and examine the statistical distribution of plausible solutions.

Although the values of $S_{h\min}$ and $S_{H\max}$ are each permitted to vary over a large range (Figure 4a), the difference between them is constrained by using a failure criterion based on J_2 (equation (3)) and therefore their difference is more robustly determined than the individual values. Figure 4b shows the distribution of permitted differences between the horizontal stresses for all of the breakouts.

We find that all viable stress solutions demand a normal faulting environment ($S_v > S_{H\max} > S_{h\min}$). Note that this result is not obvious. If the upper bound of 4.5 MPa had been used rather the values of C_0 from *Ikari et al*. [2015], 20% of the acceptable stress solutions would have been in a strike-slip regime ($S_{H\max} > S_v > S_{h\min}$). *Lin et al*. [2013] could accommodate either strike-slip or normal faulting as interpretations in part because the preliminary estimates of UCS were 6.4–7.6 MPa. The small cohesion in the laboratory tests of intact samples are an important factor that provides a tighter constraint on the current stress state in the borehole than had been available previously.

We further investigated the robustness of the result by considering non-Andersonian stress fields with the maximum principal axis inclined relative to the vertical. Utilizing the solution of *Peška and Zoback*, 1995, we find that more than 10% of the breakout widths could not be matched by any combination of far-field stresses if the inclination is greater than 10° and all of the breakouts could be satisfied with any inclination <8°. More than 90% of the breakouts can be matched if the inclination is greater than 20°. The requirement of normal faulting regime is robust.

Linearly extrapolating the inferred stress state from the breakout zone to the fault at 820 mbsf results in a resolved shear stress on the plate boundary fault plane dipping 5° to the east of 0.33 MPa, with a shear sense consistent with low-angle normal faulting; a total normal stress in the solid material of 84 MPa; and therefore an effective normal stress of 6 MPa assuming hydrostatic pore pressure (Figure 4). The resulting ratio of shear

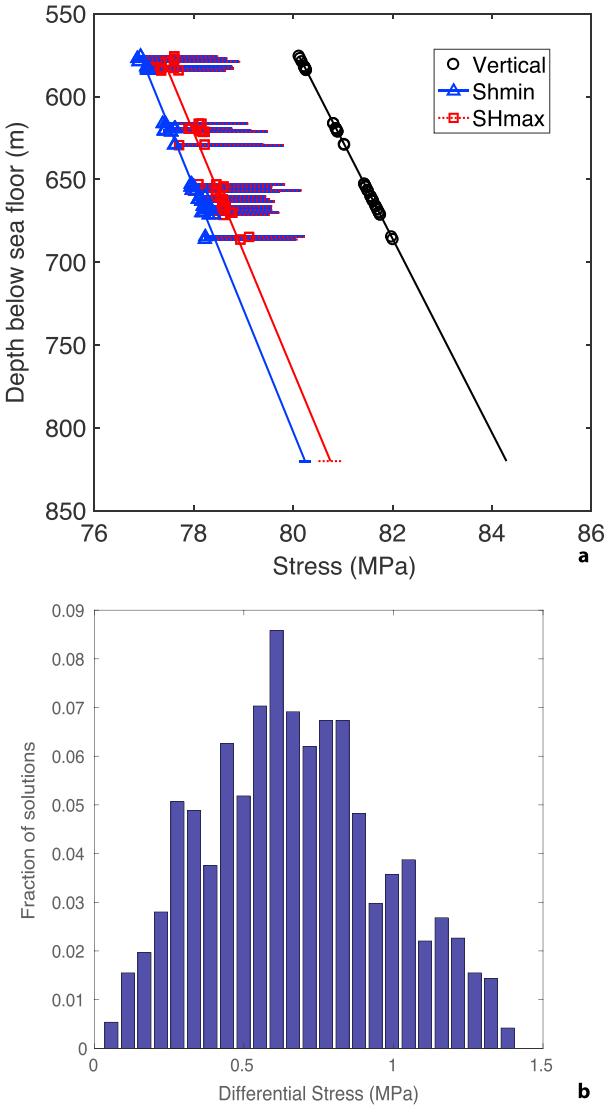

Figure 4. Combined inversion for Unit IIb. (a) Symbols indicate optimal results for each principal stress axis, and the horizontal bars mark all of the stresses that are consistent with the observed breakout width within the 2° resolution of the width measurements. Solid lines show linear best fit to optimal results and extrapolation of the trend to the depth of the 820 fault zone where no breakouts are observed. Errors marked on the extrapolation at 820 m are one standard deviation of the prediction error of the regression. (b) Distribution of all values of $S_{H\max}$-$S_{h\min}$ that are consistent with an observed breakout width within 2°. Note that the failure criterion results in a range of permissible values of $S_{H\max}$-$S_{h\min}$ that is better constrained than might be inferred from Figure 4a where the ranges of $S_{h\max}$ and $S_{h\min}$ appear to vary independently.

to normal stress is 0.06; presuming that this is a snapshot of the stress state at the end of the earthquake, it implies that this ratio (0.06) defines the fault's final friction coefficient. However, the shear stress is oriented in the opposite direction to that required for compressional stress state. Dynamic overshoot was previously inferred for the shallow portion of the Tohoku earthquake [*Ide et al.*, 2011]. Our result may also be consistent with a small amount of overshoot and, assuming that the stress drop was originally compressional, suggests complete stress drop. Alternatively, if the principal stresses are deviated (>5°) from purely vertical and horizontal [*Wang and Hu*, 2006; *Dahlen*, 1984], it would also be possible that the sign of the shear stress on the fault is positive (i.e., directed updip). The plunge of the maximum principal stress could be 8° from vertical with just as satisfactory a fit to the observed widths; therefore, there is a fundamental ambiguity in the direction of the resolved shear stress on the fault.

Regardless of the ambiguity in sign, the requirement of a near-Andersonian stress state (small deviation of the vertical stress from verticality) results in small shear stress on the fault. The frictional heat measured after the earthquake suggested that the slip-averaged coseismic friction lay between 0.05 and 0.15 (90% confidence interval) [*Fulton et al.*, 2013; *Ujiie et al.*, 2013]. Since the low-velocity coefficient of friction of the material is measured at 0.2 [*Ikari et al.*, 2015] and the coseismic value is sensitive to the average stress during the entire time of slip, it is reasonable that final value is less than the average one.

5. Lack of Breakouts Below 720 mbsf

The lack of breakouts below 720 mbsf is surprising. A simple linear extrapolation of the stress states from Unit IIb to the depth of the fault using the same procedures as before suggests that breakouts should be at least 94° wide at this depth. A pair of breakouts that encompass more than 90° of the borehole imply that more than half the perimeter has failed and is normally considered a condition for hole collapse [*Zoback*, 2007].

The drilling logs show no indication of catastrophic collapse [*Chester et al*., 2012], and the recorded annular pressures were insufficient to suppress the breakouts if the stresses and rock strength were the same as at shallower depths. Possible explanations for the lack of breakouts at these depths include (1) a change in borehole inclination, (2) a marked increase in rock strength, or (3) a change in stress state near the fault.

The first possibility could be supported by a change in borehole inclination at the base of the breakout zone. Deviated boreholes can change their stability state as they become more favorably aligned with the stress field. However, using the formulation of *Peška and Zoback* [1995], we calculate that a deviation of more than 50° is required to have a breakout width less than 90° below 720 mbsf if the stress state follows the extrapolation shown in Figure 4. Therefore, we conclude that the deviation is unlikely to explain the observed lack of breakouts.

The second possible explanation due to a change in rock strength is a plausible solution. A 20% increase in the unconfined compressive strength to 2.4 MPa (corresponding to a cohesion of 750 kPa) is sufficient to stabilize the system enough that stress states can be found that correspond to zero breakout width at depth. The highest cohesion observed in the laboratory study is only 650 kPa, but it is on the deepest sample at ~790 mbsf. Given the 400 kPa range in the cohesion data, it is plausible that higher strengths exist at depth. Such an increase in strength could potentially occur with increased compaction or cementation at depth, despite the near-fault damage. If the unconfined compressive strength is 2.6 MPa (cohesion of 800 kPa), then the extrapolation of the Unit IIb stress state to the plate boundary fault at 820 mbsf results in no breakouts. The increase in V_p measured on core samples from 2.1 at 720 mbsf to 2.4 km/s at 818 mbsf potentially supports an increased UCS and would be consistent with enhanced cementation and diagenesis in the clay-poor rocks of this interval [*Ikari et al*., 2015]. This is a plausible explanation for the observations that require no major change of stress state in the nearfield of the major plate boundary fault. However, the high-clay rocks of the fault zone would not be subject to this strengthening mechanisms and could be weak [*Chester et al*., 2013]. Therefore, further discussion is warranted.

Therefore, we consider a third explanation of a change in stress state: a reduction of the differential stress near the fault. Such a change in stress state could be a consequence of the elastically weak damage zone could supporting less deviatoric stress than the surrounding units. This option is attractive and consistent with all the data, but is not quantitatively required since no direct UCS measurements are available in the key region near the fault zone.

Note that a stress rotation in the nearfield of the fault like that suggested by *Barton and Zoback* [1994] would extend much further from the fault than observed since the rupture length of the Tohoku earthquake is more than 100 km. However, our results do concur with the Barton and Zoback conclusion of complete stress drops [*Barton and Zoback*, 1994].

6. Conclusions

Based on this reanalysis of the breakout data, we conclude the following:

1. The orientation of the maximum horizontal stress is 28° from the convergence direction. Although a parallel orientation cannot be ruled out by the data, it is not the optimal solution. The lack of consistency suggests stress changes during the earthquake comparable to the ambient stress.
2. All possible solutions of the data that utilize the laboratory constraints on strength and a 3-D failure criterion (modified Weibol-Cook) require that the system was in a normal faulting regime 14 months after the 2011 Tohoku earthquake. This is consistent with a broad range of independent observations in the region, including seafloor surveys that indicate postseismic extensional failure on presumed normal faults and normal faulting aftershocks [*Asano et al*., 2011; *Ide et al*., 2011; *Tsuji et al*., 2011]. Again, this observation implies near total stress drop.
3. Extrapolating the stress state from the breakout zone results in an effective friction on the fault that is lower than the friction averaged during all of slip.

The technical challenges of the data make certain aspects of the conclusions tentative. For instance, the breakouts cease approximately 100 m above the inferred major plate boundary fault. This observation can be explained by an increase of the strength of the rock at depth near the fault, or a reduction of

differential stress in the nearfield of the fault. In either scenario, small changes in UCS lead to very different interpretations of the stress regime. We eagerly await the possibility of returning to this region as part of the proposed IODP JTRACK project that may eventually resolve the outstanding issues and determine how the stress state may have evolved over the past several years.

All three of the major conclusions stemming from the JFAST breakout data demand a stress state incompatible with the stress state that would have favored rupture immediately before the earthquake, thus suggesting a complete or nearly complete release of the preseismic stress.

Acknowledgments
We are grateful to all of the scientists, staff, and crew of Expedition 343, the Chikyu, IODP, and CDEX without whom this expedition would not be possible. This work was supported in part by the Gordon and Betty Moore Foundation grant 3289. Data are available for download from http://sio7.jamstec.go.jp/well-logging/343/C0019B/.

References

Argus, D. F., R. G. Gordon, and C. DeMets (2011), Geologically current motion of 56 plates relative to the no-net-rotation reference frame, *Geochem. Geophys. Geosyst.*, *12*, Q11001, doi:10.1029/2011GC003751.

Asano, Y., T. Saito, Y. Ito, K. Shiomi, H. Hirose, T. Matsumoto, S. Aoi, S. Hori, and S. Sekiguchi (2011), Spatial distribution and focal mechanisms of aftershocks of the 2011 off the Pacific coast of Tohoku earthquake, *Earth Planets Space*, *63*(7), 669–673, doi:10.5047/eps.2011.06.016.

Barton, C. A., and M. D. Zoback (1994), Stress perturbations associated with active faults penetrated by boreholes: Possible evidence for near-complete stress drop and a new technique for stress magnitude measurement, *J. Geophys. Res.*, *99*, 9373–9390, doi:10.1029/93JB03359/full.

Chester, F. M., J. J. Mori, S. Toczko, N. Eguchi, and the Expedition 343/343T Scientists (2012), Japan Trench Fast Drilling Project (JFAST). IODP Prel. Rept., 343/343T, doi:10.2204/iodp.pr.343343T.

Chester, F. M., et al. (2013), Structure and composition of the plate-boundary slip zone for the 2011 Tohoku-oki earthquake, *Science*, *342*(6163), 1208–1211, doi:10.1126/science.1243719.

Colmenares, L., and M. Zoback (2002), A statistical evaluation of intact rock failure criteria constrained by polyaxial test data for five different rocks, *Int. J. Rock Mech. Min. Sci.*, *39*(6), 695–729.

Dahlen, F. A. (1984), Noncohesive critical Coulomb wedges: An exact solution, *J. Geophys. Res.*, *89*(B12), 10,125–10,133, doi:10.1029/JB089iB12p10125.

Fulton, P. M., et al. (2013), Low coseismic friction on the Tohoku-oki fault determined from temperature measurements, *Science*, *342*(6163), 1214–1217, doi:10.1126/science.1243641.

Hardebeck, J. L. (2012), Coseismic and postseismic stress rotations due to great subduction zone earthquakes, *Geophys. Res. Lett.*, *39*, L21313, doi:10.1029/2012GL053438.

Ide, S., A. Baltay, and G. C. Beroza (2011), Shallow dynamic overshoot and energetic deep rupture in the 2011 M_w 9.0 Tohoku-Oki earthquake, *Science*, *332*(6036), 1426–1429, doi:10.1126/science.1207020.

Ikari, M. J., J. Kameda, D. M. Saffer, and A. J. Kopf (2015), Strength characteristics of Japan trench borehole samples in the high-slip region of the 2011 Tohoku-Oki earthquake, *Earth Planet. Sci. Lett.*, *412*(C), 35–41, doi:10.1016/j.epsl.2014.12.014.

Jaeger, J. C., and N. G. W. Cook (1976), *Fundamentals of Rock Mechanics*, 2nd ed., Chapman and Hall, London.

Lee, H., C. Chang, S. H. Ong, and I. Song (2013), Effect of anisotropic borehole wall failures when estimating in situ stresses: A case study in the Nankai accretionary wedge, *Mar. Pet. Geol.*, *48*(C), 411–422, doi:10.1016/j.marpetgeo.2013.09.004.

Lin, W., et al. (2013), Stress state in the largest displacement area of the 2011 Tohoku-oki earthquake, *Science*, *339*(6120), 687–690, doi:10.1126/science.1229379.

Nakamura, Y., S. Kodaira, B. J. Cook, T. Jeppson, T. Kasaya, Y. Yamamoto, Y. Hashimoto, M. Yamaguchi, K. Obana, and G. Fujie (2014), Seismic imaging and velocity structure around the JFAST drill site in the Japan Trench: Low *Vp*, high *Vp*/*Vs* in the transparent frontal prism, *Earth Planets Space*, *66*(1), 121–112, doi:10.1186/1880-5981-66-121.

Peška, P., and M. D. Zoback (1995), Compressive and tensile failure of inclined well bores and determination of in situ stress and rock strength, *J. Geophys. Res.*, *100*, 12,791–12,811, doi:10.1029/95JB00319.

Tsuji, T., et al. (2011), Potential tsunamigenic faults of the 2011 off the Pacific coast of Tohoku Earthquake, *Earth Planets Space*, *63*(7), 831–834, doi:10.5047/eps.2011.05.028.

Ujiie, K., et al. (2013), Low coseismic shear stress on the Tohoku-oki megathrust determined from laboratory experiments, *Science*, *342*(6163), 1211–1214, doi:10.1126/science.1243485.

Wang, K., and Y. Hu (2006), Accretionary prisms in subduction earthquake cycles: The theory of dynamic Coulomb wedge, *J. Geophys. Res.*, *111*, B06410, doi:10.1029/2005JB004094.

Yang, T., T. Mishima, K. Ujiie, F. M. Chester, J. J. Mori, N. Eguchi, S. Toczko, and Expedition 343 Scientists (2013), Strain decoupling across the décollement in the region of large slip during the 2011 Tohoku-Oki earthquake from anisotropy of magnetic susceptibility, *Earth Planet. Sci. Lett.*, *381*(C), 31–38, doi:10.1016/j.epsl.2013.08.045.

Zoback, M. D. (2007), *Reservoir Geomechanics*, Cambridge Univ. Press, Cambridge.